Uncertainty Quantification in Internal Flows Applied to Manufacturing Tolerances

R. Nigro[1] and G. Coussement[2]
University of Mons, Mons, 7000, Belgium

D. Wunsch[3] and C. Hirsch[4]
Numeca International, Brussels, 1170, Belgium

Defining an inverse design problem, which aims at maximizing the manufacturing tolerances while keeping a small variability of the turbomachinery performances, requires methods allowing the propagation of manufacturing uncertainties. Quantification of manufacturing uncertainties requires a large number of correlated uncertainties to represent the manufacturing process. A non-intrusive probabilistic collocation method, in combination with a sparse grid formulation, is applied for a high number of uncertainties and is coupled with a principal component analysis to treat correlated uncertainties. The method is applied to the NASA Rotor 37 with correlated uncertainties on the blade geometry. The correlations are defined by an analytical function and the influence of each parameter of this function is investigated. It is shown that the modification of the amplitude of the variability allows to define an inverse robust design problem.

Nomenclature

$Cov(d)$	=	covariance between 2 points based on their distance
d	=	distance
$E[\xi]$	=	expected value of a random variable ξ
K_x	=	covariance Matrix
K_ν	=	modified Bessel function of the second kind
l	=	covariance length
M	=	number of random variables contained in the random field
N	=	number of modes kept to guarantee an error inferior to ϵ on the random field with PCA
$u\ (\vec{x}, t, \xi)$	=	non-deterministic solution
t	=	element of a topological space T
X_{dev}	=	vector of size $1xM$ containing the amplitude of deformation for each point of the surface
X_t	=	a discrete random field
$\overline{X_t}$	=	mean value for the random field
Y_i	=	vector of size $1xM$ containing the value of each random variable for a ξ_i
Γ	=	gamma function
ϵ	=	a small value defining the error allowed on the random field representation
λ_k	=	eigenvalue associated with the eigenvector ϕ_k
μ_1	=	the first non-centered moment (i.e. the mean)
μ_n	=	n centered moment (i.e. the variance for $n = 2\ldots$)
ν	=	smoothness parameter of the Matérn function
ξ	=	random variable
σ	=	standard deviation
σ^2	=	variance
ϕ_k	=	the k eigenvector of the covariance function

[1] Researcher in Fluids Machines Unit, University of Mons, remy.nigro@umons.ac.be
[2] Head of Fluids-Machines Unit, University of Mons, gregory.coussement@umons.ac.be
[3] Head of Robust Design group, NUMECA International, dirk.wunsch@numeca.be
[4] Professor and President, NUMECA International, charles.hirsch@numeca.be

I. Introduction

THE interest industry and academia for uncertainty quantification (UQ) techniques has increased over the last few years, and in particular for internal flows ([2], [8], [15]). In contrast with current design methods based on a deterministic approach, the future of the turbomachinery design needs to take into account all uncertainties, and in particular the stochastic variations of the geometry resulting from the manufacturing variability. The variation in the geometry is responsible for a variability in terms of performances (efficiency, pressure ratio,…). UQ methods allow to propagate the uncertainties and, from a given probability distribution function (PDF) of the geometrical parameters, determine the PDF of the performances. The geometry variation must be described accurately to have an accurate estimation of the performances variability: An important number of correlated uncertainties must be considered. The correlations, which describe the dependence between different uncertain variables must be considered to represent the preferential shapes of geometry deformation caused by the manufacturing process: if a blade has a variable thickness and span-height but an almost constant volume and a constant chord, the thickness and the span-height are *correlated* because an increase of the thickness means the span-height has a high probability to decrease (two dependent parameters).

These correlations need to be considered while performing the propagation of the uncertainties. However, Most of the UQ techniques, such as the non-intrusive probabilistic collocation method (NIPColM)[5], are limited to independent variables. Therefore, the principal component analysis (PCA) [9] is used in order to decorrelate the uncertainties and allow the use of UQ techniques developed for uncorrelated uncertainties. The PCA consists in solving the eigenproblem of the correlation matrix and finds a set of orthogonal vectors representing the geometrical variability . The resulting eigenvectors (which can be called modes) determine the shape of deformation of the geometry and their associated eigenvalues represent the amplitude of this deformation. as all the vectors have a different amplitude, the PCA allows to reduce the number of uncertainties by a truncation of the modes with the smallest amplitude of deformations. This helps to cope with another issue of UQ methods which is the exponential increase of the costs with the number of uncertainties. The so-called curse of dimensionality is also tempered thanks to the use of sparse grid techniques ([1], [2] and [6]).

The amplitude of deformation applied to the geometry can be modified by multiplying all the eigenvalues by a constant factor. This modification of the amplitude of deformation for a constant shape can be linked with different tolerances defined for a given manufacturing process. Therefore, a UQ study performed for different amplitude of deformations allow to determine the influence of the geometrical tolerances on the performances. This leads to the inverse robust design problem, which finds the optimal manufacturing variability, which is a trade-off between costs and performances: A high manufacturing variability causes a high variation of the perofrmances and a small manufacturing variability results in a high production cost for the product.

II. Uncertainty Quantification in turbomachinery

UQ methods provide usefull informations for the turbomachinery engineering design. Indeed, first they provide an information on the sensitivities of the performances to the input uncertainties thanks to the scaled sensitivity derivatives [16]. In addition, an information on the variability of the performances can be obtained through a reconstruction of the PDF or the use of error bars representing the mean value $+/-\sigma$. The example of the NASA Rotor 37 with 5 uncertianties is used to show the possible outputs of the NIPColM.

The scaled sensitivity derivatives ([1] and [16]) provide a measure of the sensitivity of a QoI with respect to an input uncertainty. Applying these sensitivities on a case with both operational and geometrical uncertainties may allow to discard some of the input uncertainties if they have no significant impact on the QoI. The considered uncertainties are: the inlet total pressure, the outlet static pressure, the tip clearance, the leading edge (LE) blade angle and the trailing edge (TE) blade angle.

Two uncertainty models are tested. The first model describes LE blade angle and TE blade angle as independent random variables in 3 sections of the blade (those quantities are interpolated on other span position), while the second model considers only 1 random variable for the LE blade angle and 1 random variable for the TE blade angle. It means the blade angle is multiplied by a same factor in each section.

It can be seen that, with the considered uncertainties, the span-wise discretization of the random variables has no real impact on the sensitivities of QoI (cf. fig. 1). Indeed, comparing the summed scaled sensitivity derivatives of LE blade angle and TE blade angle for the 2 models does not show an important difference (difference of 3% for the scaled sensitivity of the mass flow). Considering this, it can be stated that in this case, the use of the second uncertainty model is recommended. Moreover, the TE angle has a negligible influence on the QoI. Thus, this uncertainty can be discarded for further study. Which results in the reduction of the number of random variables from 9 to 5 [1].

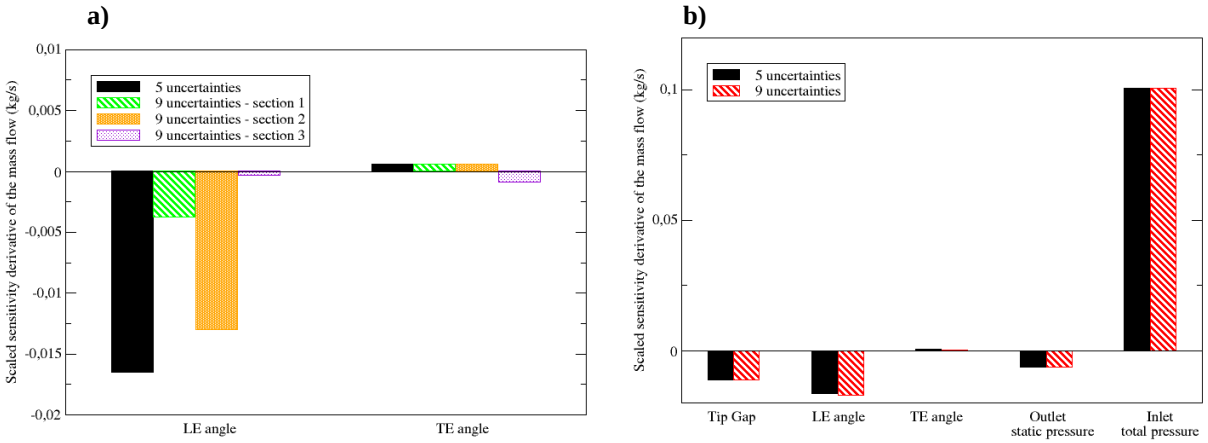

Figure 1. Comparison of scaled sensitivity derivatives of the mass flow for a model with 5 and 9 uncertainties.

A full non-deterministic performance curve can be determined thanks to the NIPColM for a given rotational speed (in the example, the rotational speed is fixed at 1800 rad/s). Non-deterministic mean and deterministic value are not identical in this case (fig. 2). Figure 3 shows clearly that a non-deterministic computation is needed to obtain the average performance of the NASA rotor 37. This difference shows a decrease of the pressure ratio and of the efficiency as a function of the mass flow when the uncertainties are considered. This decrease is about 0.5% for the pressure ratio and 0.3% for the efficiency, considering a mass flow of 20 kg/s. Moreover, the error bars give an additional information on the design.

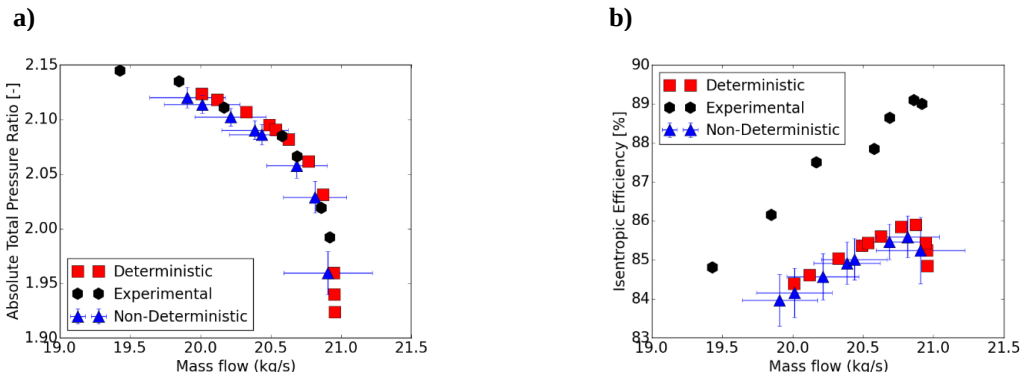

Figure 2. Comparison of deterministic and non-deterministic performance curves at 1800rad/s: (a) the pressure ratio as a function of the mass flow and (b) the efficiency as a function of the mass flow .

The full PDF can also be reconstructed based on the Pearson reconstruction method [13] and the outputs of the NIPColM. The reconstruction of the PDF for a mass flow equals to 98% of the choked mass flow, shows the interest of reconstructing the PDF. Indeed, fig. 3 shows that the representation with the mean value and an error bar of $+/-\sigma$ are misleading if they are compared with the reconstructed PDF. This is due to the use of the third statistical moment in the reconstruction method. Indeed, the third moment allows to determine the skewness of the distribution and thus its asymmetry. This asymmetry cannot be taken into account in a representation that uses mean and standard deviation.

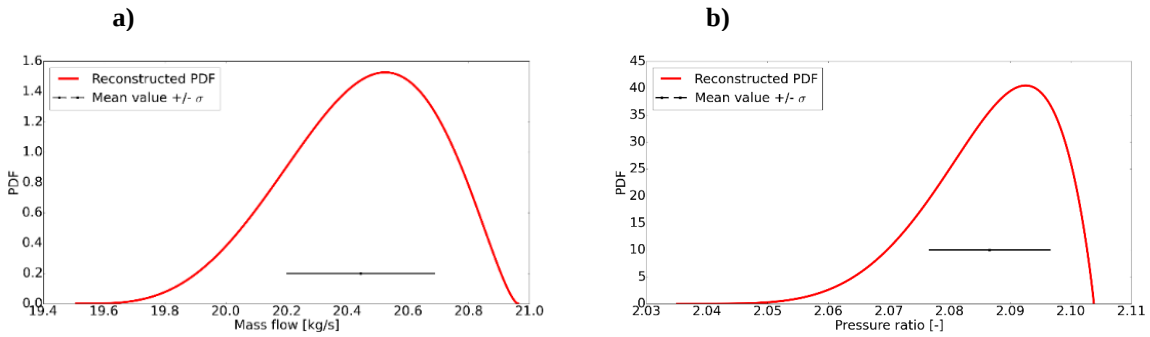

Figure 3. : Reconstructed probability density function for different QoI: (a) massflow, (b) pressure ratio.

III. Correlations on the geometry

The manufacturing uncertainties can be represented as a random field [17]. The random field is a collection of random variables which includes their dependence. The expression of a random field is given in the eq (1)*:*

$$X_t = \{\xi_t : t \in T\} \tag{1}$$

Considering the different possible topological spaces T composed by a defined number of elements t, the number of random variables contained in the random field can be either infinite (continuous random field) or finite (discrete random field). A discretized geometrical surface can be defined as a discrete random field by considering that the collection of the random variables is defined by the ensemble of the geometry points defining the discrete surface.

$$Cov(X,Y) \quad = E[(X - E[X])(Y - E[Y])] \tag{2}$$

In this work, the relative influence between random variables is limited to pairwise influence. This is the covariance, which is defined in the eq. (2)

Figure 1 shows different realisations of an airfoil by considering each surface point as an independent variable (i.e. no covariance) (fig. 4 (a)) or by defining a covariance between the surface points (fig. 4 (b)). These figures show that the random fields allow to introduce some preferential shapes of deformation on the geometry.

Random fields cannot be used directly for UQ study because of the high number of random variables they contain (200 in the example of fig. 1), and because of the covariance between random variables. Thus, the random variables contained in the random field need to be transformed.

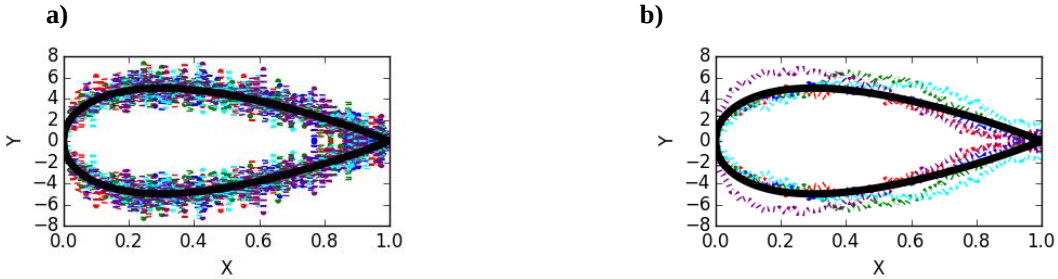

Figure 4. Realisations of an airfoil discretized with 200 points considering (a) each of these points as independent or (b) as a random field described with a covariance between each of its points (black line: nominal value; dashed lines: realisations).

IV. Treatment of correlated manufacturing uncertainties

The method used for the propagation of the uncertainties is the Non-Intrusive Probabilistic Collocation Method (NIPColM) [5]. This method is coupled with a sparse grid (SG) technique [6]. Details on the coupling between the two methods are given in [1]. The NIPColM coupled with the SG efficiently propagates the uncertainties for internal flows such as compressors: The mean and the standard deviation of a quantity of interest (QoI) are estimated with 11 CFD evaluations for 5 uncertainties and the probability density functions (PDF) are evaluated with 71 CFD runs for 5 uncertainties [2].

The NIPColM is limited to independent uncertainties, which is a major drawback for the treatment of industrial problems as they can show high correlations [7]. Therefore an extension of this method is proposed to treat the correlations: the Principal Component Analysis (PCA) (also known as Proper Orthogonal Decomposition (POD), Karhunen-Loeve Transform (KLT)) [9] is coupled with the NIPColM to decorrelate the problem thanks to a change of variables based on an orthogonal decomposition. The method to treat manufacturing uncertainties can be separated in successive steps, which are detailed hereafter:

The first step for a UQ analysis on a correlated problem is to define the correlations between the uncertainties. These correlations are summarized in a covariance matrix which describes the dependence between pairs of uncertain parameters. The uncertain parameters are the coordinates of the geometry points defining the uncertain surface. If a set of measurements of the geometry representing the manufacturing process variability is available, it is possible to compute the sampled covariance matrix [10]. Otherwise, as this kind of measurements are not always available, the covariance can be defined through an analytical function such as the Matérn covariance function (Eq. (3)) [11]. The influence of the smoothness parameter on the covariance function is shown on the figure 5. As it is shown that an increased value of the smoothness parameter quickly converges to a given function shape, in the following studies, the smoothness parameter $\nu \rightarrow \infty$, which leads to a squared exponential function (Eq. (4)). The different parameters of this equation (σ^2 and l) should be defined based on an a priori knowledge and some assumptions. The influence of each parameter is studied in the section III.

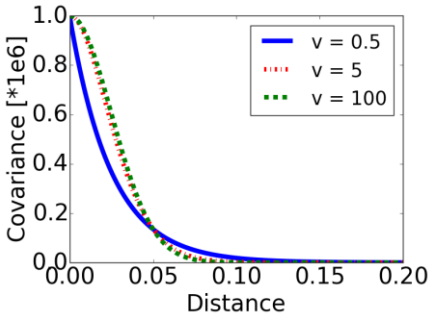

Figure 5. Differences in the covariance function as a function of the smoothness parameter.

$$Cov(d) = \sigma^2 * \frac{1}{\Gamma(\nu)2^{\nu-1}} \left(\sqrt{2\,\nu}\frac{d}{l}\right)^{\nu} K_{\nu} \left(\sqrt{2\,\nu}\frac{d}{l}\right) \quad (3)$$

$$Cov(d) = \sigma^2 * exp\,(-\frac{d^2}{2l^2}) \quad (4)$$

Then, the PCA (eq. (5)) is applied on the covariance matrix, which corresponds to solving the eigenproblem of this matrix. The resulting eigenvectors determine the modes of deformation of the geometry whereas their associated eigenvalues correspond to the amplitude of this deformation. The PCA can be represented as the determination of the orthogonal directions in which the variability is maximized. Figure 6 represents a PCA applied on a two dimensional random field represented by its realisations (the dots): The original variables are the black axes and the decorrelated variables (i.e. eigenvectors of the correlation matrix) are the purple axes.

Each eigenmode corresponds to a random variable for which the probability density function is Gaussian and centered ($\mu_1 = 0$) with a variance $\sigma^2 = \lambda$. The truncation of the number of eigenmodes is performed at this step: After sorting the eigenmodes in decreasing order of eigenvalues, N modes are kept to guarantee that the error on the random field is inferior to ϵ (Eq. (6)).

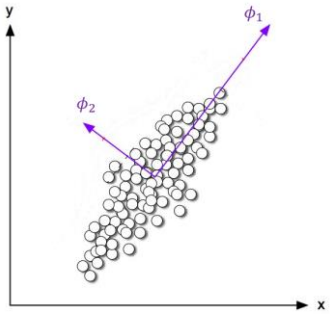

Figure 6. Principles of the PCA

$$X_t = \overline{X_t} + \sum_{k=1}^{M} \xi_k^{PCA} * \phi_k \quad (5)$$

$$\epsilon > 1 - \frac{\sum_{k=1}^{N} \lambda_k}{\sum_{k=1}^{M} \lambda_k} \qquad with\ \lambda_1 > \lambda_2 > \cdots > \lambda_M \tag{6}$$

Finally, The NIPColM is applied to the set of random variables defined with the PCA. Each collocation point defines a set of value for the set of uncorrelated random variables. A vector of deformation is obtained for each mode by multiplying the normalized eigenvector by the value defined by the collocation method. Once all the vectors of deformation are defined, the deformation of each geometrical point can be determined by performing an inverse transformation (Eq. (7)). It can be seen that the deformation defined for each point of the surface is the sum of the contribution from each modes. As X_{dev} is given considering centered random variables, this value must be added to the mean value of each point (Eq. (8)). The deformed surface is obtained by replacing the original points by their coordinates defined in $X_{notCentered}$.

$$X_{dev} = \sum_{i=1}^{N} \Phi_i \, Y_i \tag{7}$$

$$X_{notCentered} = X_{dev} + \mu \tag{8}$$

As the number of modes is limited to N, the $M - N$ remaining eigenvectors are not considered. The neglected modes are responsible for the reconstruction error. As the neglected modes induce very small deformations, their influence on the solution can be assumed to be negligible.

V. Influence of the covariance function parameters

In the case of a squared exponential covariance function (Eq. (2)), two parameters are used to determine the covariance between two geometry points: the covariance length l and the variance σ^2. Their influence is investigated on the performances of the NASA Rotor 37, a single stage compressor for which several CFD and experimental studies have been performed [12]. All the computations are performed using FINE™/Turbo [4] on a full structured multi-block mesh with 2.8 million points chosen after a mesh convergence study. A single CFD run takes approximatively 10 minutes on 16 cores to reach convergence of global quantities such as mass flow (2.67 CPU*Hours).

A. Influence of the covariance length

The covariance length represents the distance in-between two geometrical points for which a non-negligible correlation exists. Changing the covariance length changes the shape of the covariance function (fig. 7). For a smaller value of the covariance length, the covariance function decreases more quickly according to the distance. This means that with a smaller covariance length value, the correlation between a given pair of points is also smaller. Two values of this parameters are tested in order to determine their impact on the performances of the Rotor 37. The first case has a covariance length of 0.05m which corresponds to 100% of the chord while the second case uses 0.025m for this parameter, which corresponds to 50% of the chord length.

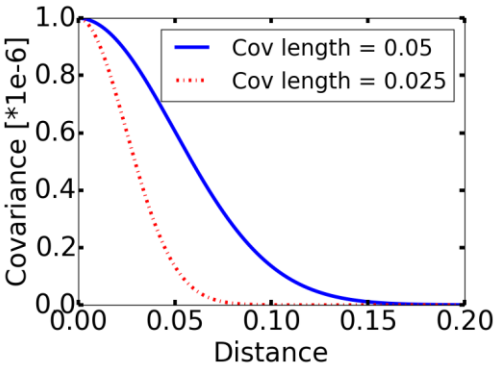

Figure 7. Differences in the covariance function according to the "covariance length" parameter.

This difference in the covariance function has an impact on the modes: the shape and the amplitude of deformation changes completely for these different covariance length values. For high covariance lengths, the first few modes are sufficient to represent the deformation of the geometry caused by the uncertainty as the cumulative energy grows quickly with the number of modes. Therefore, the truncation performed by the PCA results in a small number of modes (fig. 8). On the opposite, small covariance length means that the PCA truncation cannot discard lots of modes as the relative importance of the first few modes in the total deformation is small. In the extremum case of a

covariance length of 0, the uncertainties are considered as independent and thus very wavy shapes are possible and if the covariance length is infinite, the resulting uncertainty is represented with 1 mode corresponding to a translation applied on all the geometrical point. The number of modes *N* kept for this case is of 5 for the covariance length of 0.05m (11 CFD runs for the mean and the standard deviation and 71 for the PDF shape) and 12 for the covariance length of 0.025m 05m (25 CFD runs for the mean and the standard deviation and 337 for the PDF shape).

This parameter has an influence on the performances such as the pressure ratio (fig. 9 (a)) and the isentropic efficiency (fig. 9 (b)). The PDF reconstructed based on the first four statistical moments (Pearson reconstruction method [13]) shows that the mean value does not change slightly (max. 0.027%) but the variance changes of almost a factor 2 for the pressure ratio and a factor 10 for the efficiency, the variance is the highest for the small values of the covariance length.

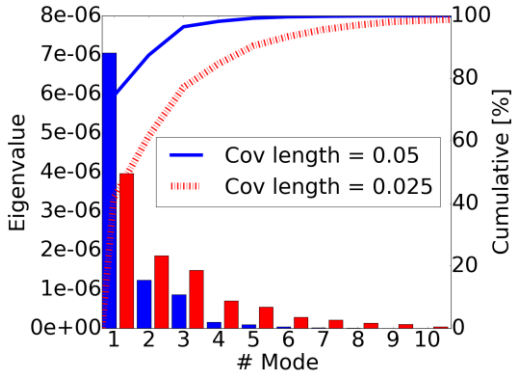

Figure 8. Differences in variation of geometry inherent to each mode regarding to the "covariance length" parameter.

a) **b)**

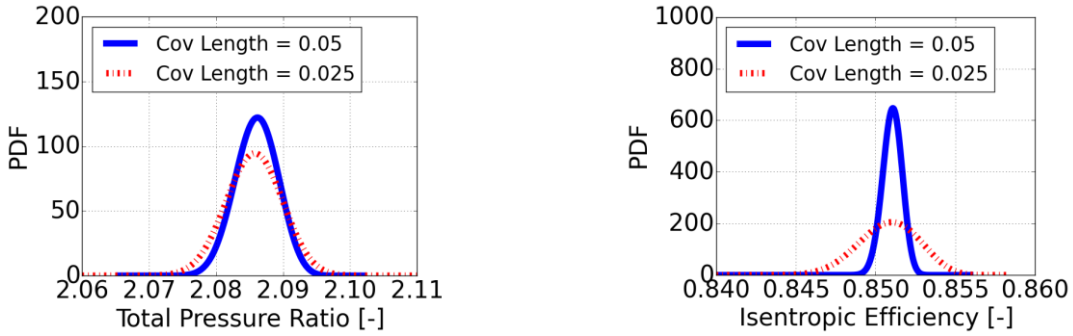

Figure 9. PDF reconstruction for the pressure ratio (a) and the isentropic efficiency (b) for 2 values of the covariance length parameter.

B. Influence of the variance

The variance parameter represents the amplitude of deformation associated with the covariance matrix. Therefore, changing this parameter results in changing the maximal deformation associated with each eigenmode while keeping their shape unchanged [14], which is shown by the comparison of the covariance functions for two different value of this parameter (variance equals 1^{-8} or 1^{-6}). These two functions only differ by a scaling factor identical to the ratio between the two parameter values (fig. 10 (a)). As a result, the PCA truncation is insensitive to the variation of this parameter. Indeed, the relative cumulative distribution of the amplitude of deformation is identical for the different values of this parameter (fig. 10 (b)).

a) **b)**

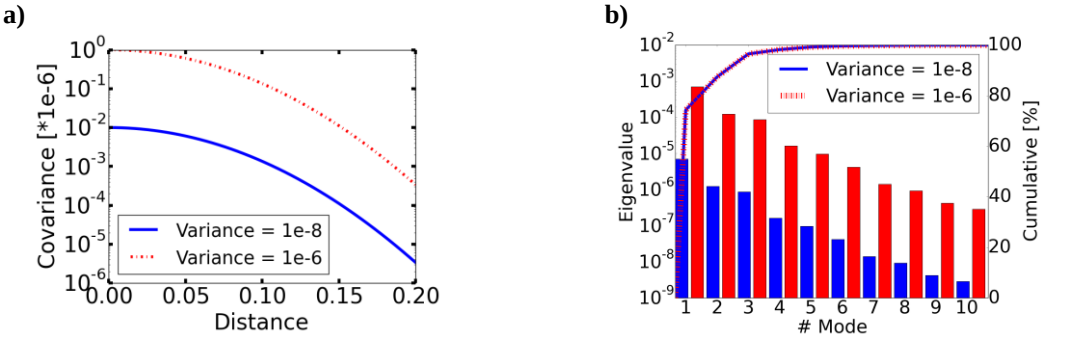

Figure 10. Comparison of the covariance function (a) and the eigenvalues of each modes (b) for two different values of the variance parameter (Rem: the two graphs have a logarithmic abscissa)

This parameter has also an impact on the Rotor 37 performances. The influence can be shown from the scaled sensitivity derivatives (s) of a quantity of interest (u) with respect to a random variable ξ ($s = \sigma * \frac{\partial u}{\partial \xi}$) [16]: For both the pressure ratio and the efficiency, the ratio between the two values of the scaled sensitivities is close to 10, which is the ratio between the two standard deviations and the most influential mode is not necessarily the mode responsible for the most important deformation (fig. 11 (a and b)). As the scaled sensitivities and the standard deviation are multiplied by the same ratio, it can be concluded that the derivative is kept constant. The same observation can be performed based on the reconstructed PDF in which it can be seen that the interval of variation changes by approximatively a factor 10 (fig. 12 (a and b)), which is also the ratio between the standard deviation of the QoI (the efficiency and the pressure ratio). This observation shows that the response surface of the pressure ratio with respect to each uncertainty follows a linear behavior, within the range of variability of the surface. This might not be the case for a higher amplitude of deformation or for a different covariance function.

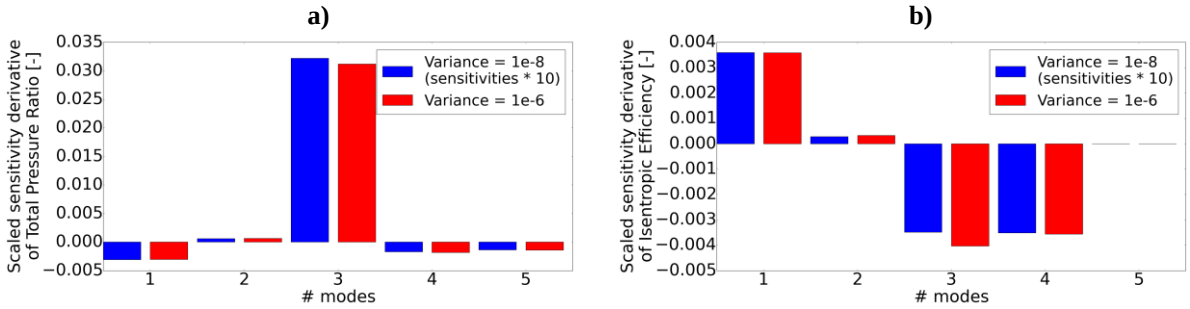

Figure 11. Scaled sensitivity derivatives for the pressure ratio (a) and the isentropic efficiency (b) for 2 values of the variance parameter (scaled sensitivity derivatives of the case with a variance of 1e-8 (blue bars) are multiplied by 10 for a comparison purpose).

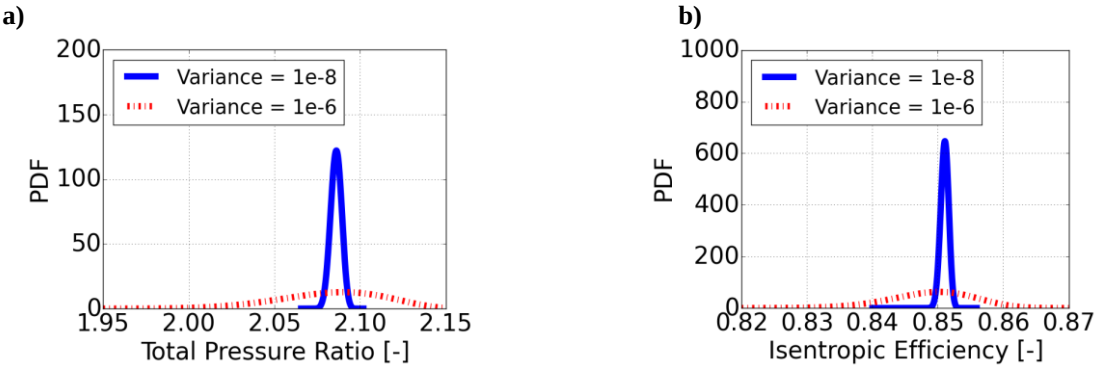

Figure 12. Reconstructed PDF for the pressure ratio (a) and the isentropic efficiency (b) for 2 values of the variance parameter.

VI. Towards inverse robust design

A. Inverse Robust Design concepts

The variation of the performances caused by a change of the variance parameter allows to define an *inverse robust design* problem. Indeed, in opposition to the robust design, which consists in determining the design which minimizes the influence of the uncertainties on the performances for a defined set of uncertainties, the inverse robust design aims at determining the maximal variability of the input uncertainties which allows to keep a given minimal performance. This concept can be used for turbomachinery designs to define the manufacturing tolerances which can be applied on the blade to guarantee a given minimal efficiency.

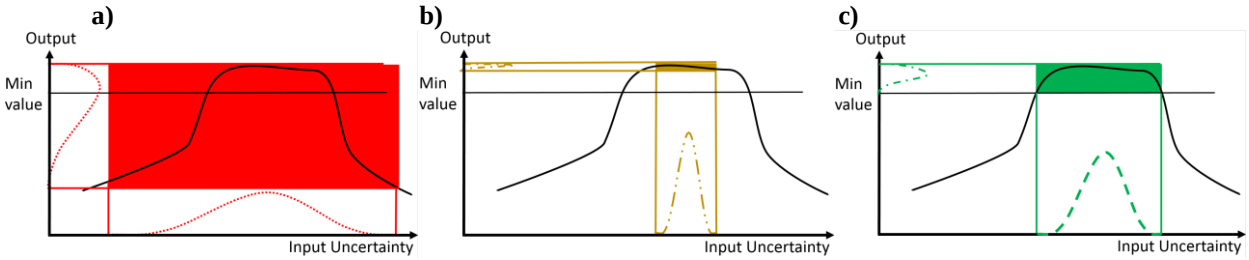

Figure 13. Concept of inverse robust design and tolerancing: (a) The tolerancing is too loose (the minimal value of the output is inferior to the minimal acceptable value), (b) the tolerancing is too thigh (the minimal value of the output is superior to the minimal acceptable value) and (c) the tolerancing is optimized (the minimal value of the output is the minimal acceptable value).

This concept is illustrated with a case of one performance value depending on one uncertainty for which the variability must be determined (fig. 13). This example shows that having loose tolerances may result in a non-optimal product as the variability results in a loss in terms of performances (fig. 13 (a)). On the opposite, tight tolerances results in an increased manufacturing cost and thus, even if the performances meet the requirements, the product cost is increased and it is thus not an optimal design (fig. 13 (b)). Therefore, an efficient definition of the variability has the largest possible variability ensuring the minimal required performances (fig. 13 (c)). The design shown in fig. 10 (c) corresponds to the result of an inverse robust design problem as the variability of the input is maximized and the requirement is fulfilled (min value determined by the black line in fig. 13).

B. Inverse Robust Design of the Rotor 37

The manufacturing uncertainties considered on the Rotor 37 are defined through a covariance function with a covariance length of 0.05m and a variation of the variance parameter in order to determine its influence on the efficiency of the single stage compressor. The objective is to find a trade-off between the minimal efficiency for which there are 90% of probability to have a higher efficiency (i.e. the quantile $P_{0.9}$) and the value of the variance parameter.

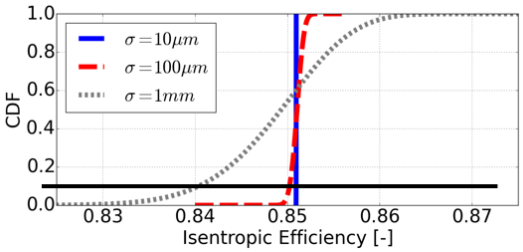

Figure 14. Cumulative distribution function of the efficiency for three different values of the standard deviation of the

The reconstruction of the cumulative distribution function (CDF), which is the integral of the PDF, allows a simple visualization of the quantile (fig. 14). Indeed, the CDF is a bijection between all the possible efficiency values and the interval [0, 1], which corresponds to the cumulative probability. Therefore, the efficiency value corresponding to a cumulative probability of 0.1 means that the probability to have a smaller efficiency is 10% and in extension, the probability of having a higher efficiency is 90%. The determination of these quantiles is performed for different values of the variance parameter corresponding to a standard deviation of respectively 10 µm, 100 µm, and 1mm. The minimal efficiency value with a probability of 90% is of 0.8404 for a standard deviation of 1mm and by reducing this standard deviation of a factor 10 (standard deviation of 100 µm) this minimal value increases up to 0.8502, which is an interesting gain. The reduction of the standard deviation to 10 µm only increases the minimal efficiency to 0.8509, which seems a high price to pay in for a small efficiency increase. It seems the best tolerancing for the given deformation shape is a standard deviation of 100 µm.

Table 1. Differences in variation of geometry inherent to each mode regarding to the "covariance length" parameter.

Standard Deviation	$1\ mm$	$100\ \mu m$	$10\ \mu m$
$\boldsymbol{P_{0,9}}$	84,04%	85,02%	85,09%

The differences in the 0.9 quantile of the efficiency can be explained by the influence of the manufacturing variability on the flow. Figure 12 shows the Mach number at 90% of span height for the 3 different variabilities for a minimal value of the third mode, which is the most influential mode on the efficiency (fig. 11 (b)). The case with a standard deviation of 1mm is characterized with a stronger shock than the two other cases all over the span height (fig. 15, 16, and 17). Figure 17 (at 90% span height) shows a detached boundary layer after the shock on the suction side for the variability of 1mm while the two other cases have a non-detached boundary layer. This difference is most likely responsible for the difference observed in terms of efficiency. It can be deduced that in this case, solving the inverse design problem corresponds to the determination of the maximum variability of the manufacturing uncertainties keeping an attached boundary layer near the tip of the blade.

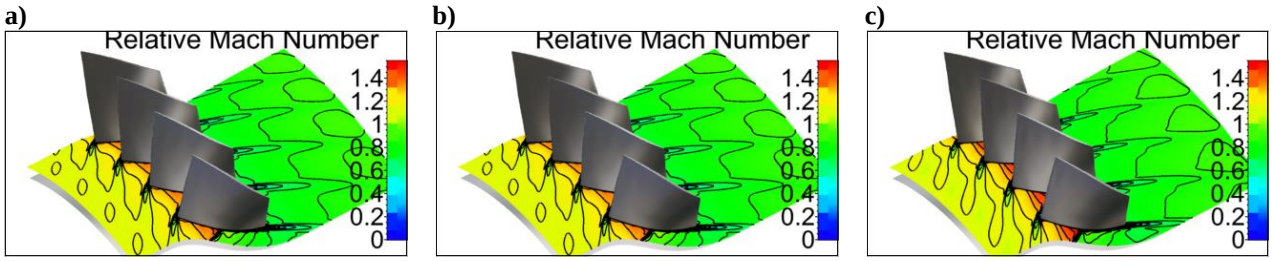

Figure 15. Mach number at 10% of span height for the minimal value of the third mode with a varying standard deviation: (a) $\sigma = 10$ μm, (b) $\sigma = 100$ μm, (c) $\sigma = 1$ mm.

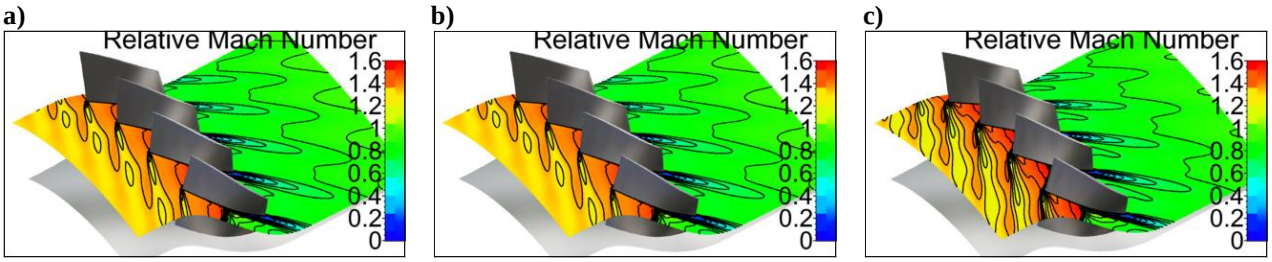

Figure 16. Mach number at 50% of span height for the minimal value of the third mode with a varying standard deviation: (a) $\sigma = 10$ μm, (b) $\sigma = 100$ μm, (c) $\sigma = 1$ mm.

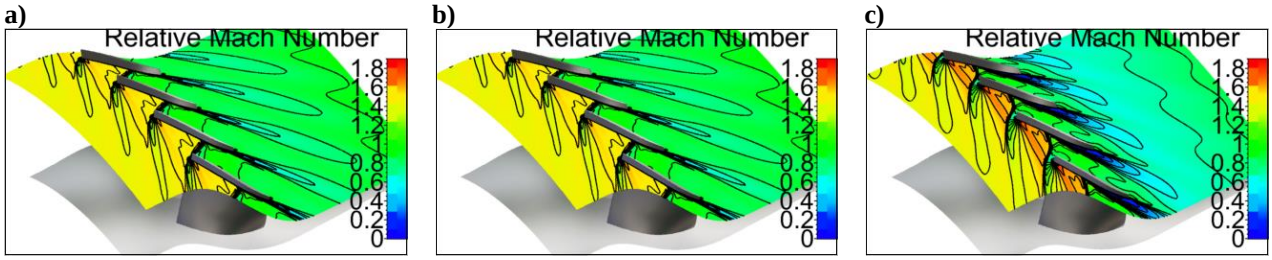

Figure 17. Mach number at 90% of span height for the minimal value of the third mode with a varying standard deviation: (a) $\sigma = 10$ μm, (b) $\sigma = 100$ μm, (c) $\sigma = 1$ mm.

The comparison of the radial profiles of the efficiency (fig. 18) shows that the highest variability for the case with a standard deviation of 1 mm is near the tip of the blade. This can be explained by the detached boundary layer shown in fig. 17 (c). The two other tested standard deviations show variations of the efficiency which are not significant. The analysis of the radial profiles corroborates our previous analysis and the standard deviation of $100\mu m$ can be determined as the optimal manufacturing variability.

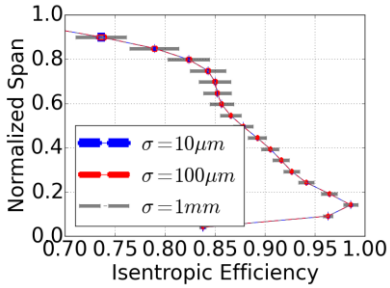

Figure 18. Radial profiles of the efficiency for different amplitude of deformation (error bars =+/- 6 σ).

This test case shows that an inverse design method can be applied to determine the manufacturing tolerances of a compressor blade. This test is based on the test of some discrete values of variability, which can be linked to different tolerance grades. The tolerance can thus be determined amongst the tested variabilities. The method can also be coupled with an optimization algorithm in order to find the best variability given a required minimal efficiency. In the case tested, the deformation shape is independent from the amplitude of the variability. The method can be extended without any limitations to varying shapes by solving the eigenproblem for each tested amplitude of variation.

VII. Conclusion

The coupling of the non-intrusive probabilistic collocation method with the principal component analysis allows the treatment of correlated uncertainties. This method is successfully applied to the single stage compressor NASA Rotor 37 with uncertainties on the geometry of the blade described with covariance on the points of the surface. The covariance matrix is defined thanks to a squared exponential covariance function and depends on two parameters which are the covariance length and the variance.

The influence of both parameters has been assessed through the analysis of the resulting probability density function, the scaled sensitivity, the shape of the covariance function, and the relative influence of each mode in the overall deformation. The covariance length, which represents the distance on which two points have an influence on each other, changes completely the shape of deformation and the relative influence of each mode. The higher it is, the smoother is the geometry deformation and therefore the smaller is the variability of the quantities of interest. The variance parameter gives information on the maximal amplitude of deformation and has no influence on the shape of deformation. For the covariance function studied, a change of a factor 10 for this parameter results in a change of approximatively the same factor for the variability of the quantities of interests (efficiency and pressure ratio). This means that for the covariance function studied, the relation between the value of this parameter and the quantities of interest is almost linear. This may not be the case for higher variances or different covariance functions.

The variation of the variance parameter, which only changes the amplitude while keeping the shape of deformation unchanged, allows to define an inverse design problem in which the objective is to find a trade-off between the minimal efficiency with a probability of 90% and the variance parameter (σ^2), which is linked to the manufacturing tolerances. The test of three different values of this parameter showed that a standard deviation (σ) of 100 µm gives a good trade-off between the two objectives (maximizing the efficiency and the tolerances). This standard deviation corresponding to this manufacturing process is determined for a defined analytical covariance function. Therefore, results with other covariance function may differs. The inverse design method proposed can be coupled with an optimization environment to automatize the search of the optimal tolerance.

Acknowledgments

The research leading to these results was partially supported by the European Union's Seventh Framework Programme (2007-2013) under grant agreement 605036, UMRIDA project.

References

[1]Wunsch D., Nigro R., Coussement G., Hirsch C., "Quantification of combined operational and geometrical uncertainties in turbo-machinery design", *Proceedings of the ASME GT2015*, GT2015-43399, 2015

[2]Wunsch D., Nigro R., Coussement G., Hirsch C., Takekoshi Y. , "Uncertainty quantification of simultaneous operational and geometrical uncertainties in turbomachinery design practice", Proceedings of the GTSJ IGTC, 2015

[3]Dunham J., CFD validation for propulsion system components, *AGARD-AR-355*, 1998

[4]FINE/Turbo, Software Package, Ver. 11.1, *NUMECA International*, Brussels, Belgium, 2016

[5]Loeven G.J.A., "Efficient Uncertainty Quantification in Computational Fluid Dynamics", *PhD thesis at Delft University of Technology*, Delft, the Netherland, 2010

[6]Smolyak S., "Quadrature and Interpolation formulas for tensor products of certain classes of functions", *Dokl. Adad. Nauk* USSR B, 240-243, 1963

[7]Lange A., Vogeler K., Gümmer V., Schrapp H., Clemen C, (2009), Introduction of a Parameter Based Compressor Blade Model for Considering Measured Geometry Uncertainties in Numerical Simulation., *ASME paper* n° GT 2009-59937

[8]Lange A., Voigt M., Vogeler K., Gümmer G., Johan E., Schrapp H., (2010), Probabilistic CFD simulation of a high- pressure compressor stage taking manufacturing variability into account, ASME paper n° GT2010-22484

[9]Loève M., "Probability theory I*", Springer-Verlag*, New York-Heidelberg, fourth edition, Graduate Texts in Mathematics, Vol. 45, 1977

[10]Johnson R. A., Wichern D.W., "Applied multivariate statistical analysis", *Pearson Prentice Hall*, 2007
[11]Rasmussen C.E, Williams C.K.I., Gaussian Processes for Machine Learning, the MIT Press, 2006
[12]Dunham J., "CFD validation for propulsion system components", *AGARD-AR-355*, 1998
[13]Elderton W. P., "Frequency-Curves and Correlation", *Charles and Edwin Layton* (London), 1969
[14]Nigro R., Wunsch D., Coussement G., Hirsch C., "Uncertainty Quantification in Internal Flows", *Application of Sensitivity Analysis and Uncertainty Qualification to Military Vehicle Design*, STO-TR-AVT-191, 2016
[15]P. Seshadri, G. Parks, and S. Shahpar., "Density-Matching for Turbomachinery Optimization under Uncertainty", *ArXiv e-prints*, October 2015.
[16]Turgeon E., Pelletier D. and Borggaard J., "Applications of continuous sensitivity equations to flows with temperature-dependent properties", *Numerical Heat Transfer 44*, 611–624, 2003
[17]Adler R.J., Taylor J.E., "Random Fields And Geometry", *Springer Monographs in Mathematics*, Springer-Verlag New York, 2005
[18]